

Landslides (2020) 17:1177–1190  
 DOI 10.1007/s10346-020-01359-w  
 Received: 31 October 2019  
 Accepted: 21 January 2020  
 Published online: 31 January 2020  
 © Springer-Verlag GmbH Germany  
 part of Springer Nature 2020

S. Martino · B. Antonielli · F. Bozzano · P. Caprari · M. E. Discenza · C. Esposito · M. Fiorucci · R. Iannucci · G.M. Marmoni · L. Schilirò

## Landslides triggered after the 16 August 2018 $M_w$ 5.1 Molise earthquake (Italy) by a combination of intense rainfalls and seismic shaking

**Abstract** On 16 August 2018, a  $M_w$  5.1 earthquake occurred in the Molise region (Central Italy) during an intense rainfall event which cumulated up to 140 mm in 3 days. Within 5 days after the seismic event, 88 landslides were surveyed and classified in disrupted and coherent as well as in first-time failures and reactivation. As it resulted by the inventorying, most of the surveyed ground effects were represented by coherent landslides involving clays, marly clays, and cover deposits on low dipping slopes. A spatial distribution analysis of landslides in relation to seismic action and rainfall intensity was carried out to evaluate the possible contribution of both the rainfall-induced saturation and the earthquake shaking to landslide triggering. Based on this analysis, in the epicentral area, it is not possible to clearly split the role of seismic and hydraulic destabilising actions, while, at greater distances, the joined contribution of rainfall and earthquake shaking could have promoted slope failures. Comparisons among collected data and existing worldwide catalogues allow to highlight, through the analysis of the spatial distribution of the surveyed landslides, the possible and not negligible effect of soil saturation during the seismic shaking both in epicentral distance vs. magnitude distribution and in number and spatial concentration of triggered ground effects.

**Keywords** Earthquake-induced ground effects · Landslides · Rainfall · Earthquake · CEDIT catalogue

### Introduction

Earthquakes are the primary worldwide cause of multiple-occurrence regional landslide events (MORLEs, Crozier 2005). MORLEs are triggered in response to a complex interaction between several factors that include climate features, local geological setting, slope geometry, landslide properties, and areal distribution of seismic shaking. The regional pattern of landslide distribution is controlled by the aforementioned factors (Nowicki et al. 2014) and the concurrent occurrence of seismic ground motion and other destabilising actions (i.e. soil saturation due to rainfall) is a fundamental topic to assess landslide hazard and associated risk to settlements and infrastructure. By their nature, MORLEs shall be investigated over large areas, where the representation of the triggering forces and induced effects allows to depict multi-hazard scenarios.

The spatial distribution of earthquake-triggered landslides (EQTLs) represents the result of a complex combination and interaction of several aspect characterising the type and magnitude of seismic trigger and ground motion (Keefer 1984; Jibson 2007; Meunier et al. 2007; Nowicki et al. 2014; Gorum and Carranza 2015) and many controlling or preparatory factors related to

geomorphological, lithological, and hydrological features (Tanyas et al. 2017; Fan et al. 2019; Valagussa et al. 2019).

The multiple combination of these factors strongly controls the frequency-size distribution of EQTL (Alfaro et al. 2012), whose density reflects through a power law correlation the severity of the earthquake (Malamud et al. 2004). The latter, expressed in terms of magnitude ( $M_w$ ) or Arias intensity, are also key factors controlling co-seismic displacement (Jibson 1993) and the maximum extent of area affected by landslides in a region or, in other words, the maximum distances where the farthest induced effects can be expected (Keefer 1984; Rodriguez et al. 1999).

Despite most of earthquake-induced landslide inventories respond to empirical relations of  $M_w$  vs. number of landslides (Keefer 2002) and  $M_w$  vs. maximum expected distance of landslides, a number of case studies report anomalous distribution or outliers with respect to the upper bound limit, due to specific failure mechanisms (Gorum et al. 2014), local seismic amplifications (Bozzano et al. 2008b; Bozzano et al. 2010; Delgado et al. 2011; Del Gaudio et al. 2014; Martino et al. 2016), and low seismic attenuation (Jibson and Harp 2012; Delgado et al. 2015). Peculiar morphological or geological site-conditions can result in marked differences in pattern of failure with respect to what expected by global empirical relations, as revealed for disrupted landslides on Italian CEDIT catalogue (Martino et al. 2014) and confirmed after Central Italy seismic sequence (Martino et al. 2019).

In addition to these factors, the predisposing contributions of rainfall prior to or directly after the earthquake were rarely analysed (Sassa et al. 2007; Wang et al. 2007; Faris and Wang 2014). Heavy rainfall able to induce a pore pressures increase within the slope can affect the local equilibrium between acting and resisting forces, favouring co-seismic shallow slope failures (Fan et al. 2019). In this sense, according to Sassa et al. (2007), the transient increase in pore pressure together with amplification of ground accelerations at the sliding surface represented the main factors controlling the 2006 Leyte landslide. The event involved a volcanoclastic cover, which failed after a small ( $M_w$  2.6) nearby earthquake occurred after heavy rainfall (571.2 mm cumulated over 5 days). Similar mechanisms of sliding-surface liquefaction were inferred by the same authors for  $M_w$  6.8 Higashi-Takezawa earthquake. Despite experimental evidences, the earthquake triggering of Leyte is still debated in landslide and earthquake researcher's community because of the low ground motion relating the earthquake to landslide-induced ground shaking (Suwa 2006). Faris and Wang (2014), by a stochastic slope stability analysis of the Tandikat landslide (West Sumatra), infer that rainfall conditions significantly rises the probability of shallow slope failure. However, because of the lack of complete and detailed landslide inventories referred to landslides induced by earthquake under saturated soil

conditions, deep insights on this topics and assessment of causes controlling landslide scenarios after earthquake are arduous.

Therefore, with the aim of contributing to the understanding of how combined and transient destabilising actions could induce slope failure, a high-resolution field surveying of landslides occurred after the 2018  $M_w$  5.1 Montecilfone earthquake (Molise, Italy) was performed. The study area also experienced before and during the seismic event intense rainfall in the epicentral area. Intensity and distribution of rainfall and seismic actions were thus framed, focusing the analyses on the potential predisposing role of rainfall in the observed distribution of EQtLs.

### Geological and geomorphological setting of the study area

The 16 August 2018 Montecilfone earthquake ( $M_w$  5.1) struck an area located in the NE portion of the Molise Region, which covers about 1000 km<sup>2</sup>, enclosed between the Frentani Mountains and the Adriatic Sea (Fig. 1). The area affected by the seismic sequence is characterised by gentle hilly reliefs with an elevation up to 1017 m a.s.l. and river valleys of variable extension, and partly belongs to the lower course of the Biferno River, while the northern and southern sectors respectively include the Trigno and Fortore River basins.

The study area is located in the easternmost sector of the Central Apennines, which is characterised by a thrust and fold structure, formed by a series of tectonic units organised in NE-verging folds, locally covered by thrust-top deposits and successions of late Miocene and Pliocene clastic units (Vezzani et al. 2004; Patacca and Scandone 2007; Vezzani et al. 2010). Such a structure is the result of early Miocene to Pleistocene shortening of collisional margin, caused by convergence of European plate and Africa-Adriatic plate (Casnedi 1978; Parotto and Praturlon 2004; Patacca and Scandone 2007).

From the structural point of view (Rapisardi 1978), the external sector of the Central Apennines is the result of a polyphasic tectonics connected with the structuring of Apennine chain that involved both superficial and deeper tectonic units deriving from deformation of the buried Apulian domain (Ricchetti et al. 1988; Patacca et al. 1992; Gambini and Tozzi 1996; Corrado et al. 1997; Scrocca and Tozzi 1999; Di Bucci et al. 1999; Patacca and Scandone 2007) and led to the definition of the current regional morphostructural setting (Corrado et al. 1997; Di Bucci et al. 1999).

In the studied area, a thick Cenozoic marine succession ascribable to the Lagonegrese-Molisan Basin widely outcrops (Vezzani et al. 2004; Patacca and Scandone 2007). The lower part of these sequences is mainly made of scaly clays with subordinate calciturbiditic intercalations and then followed by neogenic flysch composed of arenaceous-marly and calcareous-marly deposits (Vezzani et al. 2004). These successions underlie evaporitic deposits and chaotic terrain (Vezzani et al. 2004; Patacca and Scandone 2007), while the foredeep domain is characterised by a thick Plio-Pleistocene siliciclastic sequence (Vezzani et al. 2004; Calamita et al. 2011). Since the middle Pleistocene, the here considered sector was affected by a moderate tectonic uplift (Ciaranfi et al. 1983; Doglioni et al. 1994; Spalluto and Moretti 2006; Ascione et al. 2008) which led to the formation of regressive deposits and terraced marine deposits (Ciaranfi et al. 1988). Both chain and foredeep sequences are covered by continental, transitional and marine quaternary deposits, which reach some tens of metres close to the Adriatic coast (Cinque et al. 1993; Vezzani et al. 2004; Aucelli et al. 2009).

### Data and methodology

The Italian Molise region is characterised by a very high number of landslides (IFFI Project, APAT 2007). In fact, over an area of about 4461 km<sup>2</sup>, more than 28,000 landslides of variable size and characteristics can be detected (Aucelli et al. 2001; Roszkopf and Scorpio 2013; Borgomeo et al. 2014; Pisano et al. 2017).

In the study area (see Fig. 1), over 7100 landslides have been inventoried so far, whose areal size range between 100 m<sup>2</sup> and 3 km<sup>2</sup>. Dormant landslides are about 72% of the total number, while active and stabilised are respectively 24% and 4% (IFFI and Geoservizi S.r.l. database). Landslides mainly show low to very low velocity and can be classified as flows, slides, and complex earth phenomena (Hungri et al. 2014). Moreover, the gently dipping slopes are also characterised by soil creep and/or solifluction. The high landslide concentration in the study area is strictly related to lithological and geo-structural features. In such a context, gravity-induced deformations mainly involve quaternary cover deposits and the more shallow and weathered portions of the bedrock, while deep phenomena involving thick sequences of clays and marls affect considerable sectors of the coastal areas (e.g. Petacciato and Vasto landslides; Fiorillo 2003; Della Seta et al. 2013; Miccadei et al. 2019).

In the days after the Montecilfone earthquake, a total of 88 ground effects were observed and inventoried, according to the Italian catalogue of earthquake-induced ground failures database (CEDIT) criteria (Fortunato et al. 2012). Typology and style of the inventoried landslides were defined (Fig. 3), also distinguishing it between coherent and disrupted types (Keefer 1984).

The collected evidences were geo-localised during the field activities and then verified by photointerpretation following the same survey criteria of Martino et al. (2017) and Martino et al. (2019) that were focused on the distinction of clear evidences for landslide (re)activation. In this regard, specific field evidences of recent landforms (e.g. fresh scarps and cracks, slope bulging, presence of chaotic deposits) were considered for different landslide mechanisms, with the aim of deriving reliable information in view of the following earthquake/rainfall triggering interpretations. The landslides inventory was checked through a change detection analysis performed on available satellite images acquired before and immediately after the seismic and meteorological events. Afterwards, all surveyed landslides were compared with available landslides catalogues (e.g. IFFI) to assess the number of landslide reactivations with respect to first-time occurrences (Hutchinson 1988). The reactivation of already existing landslides was also evaluated on the basis of field surveys for those ones that were not previously catalogued (because of their age).

Intensity and return period of the 14–17 August 2018 rainfall event were evaluated from a dataset available for 11 thermo-pluviometric stations operating in the study area and managed by the Molise Region civil protection. However, due to the temporal overlap between seismic and rainfall event, a univocal detection of a trigger factor is challenging. Furthermore, the short duration of the rainfall event with respect to the revisit time of the available satellite images did not allow performing remotely sensed surveying to evaluate the rainfall role in landslide triggering.

However, in the following chapters, data available and the methods adopted are presented and discussed to assess possible contribution of the two triggering factors in the inventoried slope failures. Relative ratios between first-time occurrence of landslides

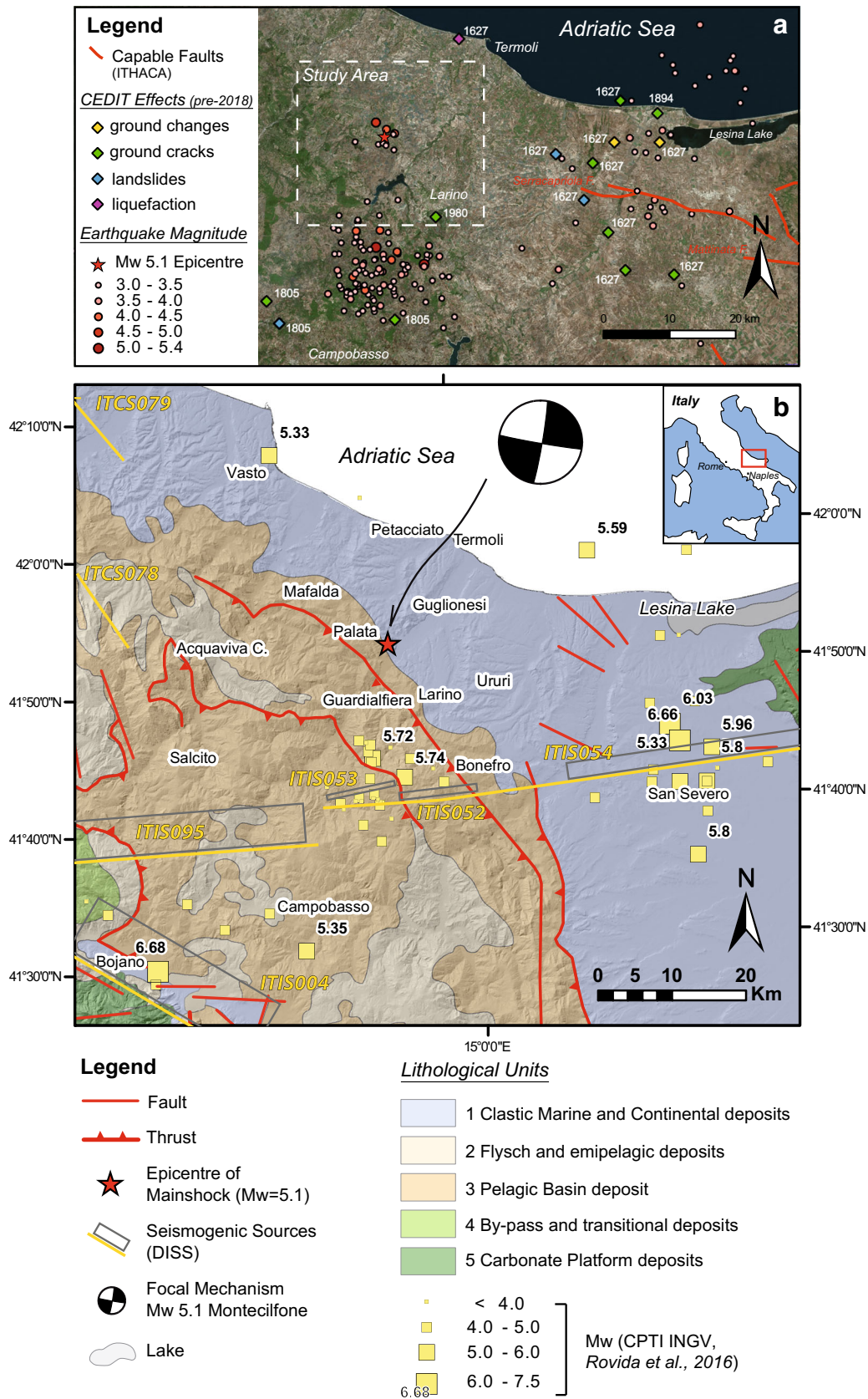


**Fig. 1** a Historical instrumental epicentres registered in the surroundings of the study area between 1985 and 2019 (red circles; <http://terremoti.ingv.it>) with pre-2018 location of earthquake-induced ground effects by CEDIT catalogue. Traces of ITHACA Active and Capable Faults are also reported. b Simplified geo-structural sketch of the study area (Triento Geological Map 1:50,000 CARG). Epicentre and focal mechanism of mainshock related to the 16 August seismic sequence of Montecifone (mainshock  $M_w$  5.1) are also reported. Locations and magnitudes of historical earthquakes in the area according to the CPTI15 catalogue (Rovida et al. 2016) and Individual Seismogenic Sources from DISS catalogue (version 3.2.1; 2018) are also shown

and reactivations were discriminated with respect to their epicentral distance and comparing it with both PGA and cumulated rainfalls experienced in the place where ground effects occurred. Such proportion and relative spatial distribution of all types of ground effects added specific details aimed to better frame the possible combined action of multiple destabilising actions controlling the EQtL scenarios.

### The 16 August 2018 Molise earthquake

On 16 August 2018, a  $M_w$  5.1 earthquake occurred at 18:19:04 UTC in Montecilfone (CB) Molise region (Central Italy) and represented the mainshock of a seismic sequence beginning 25 April 2018 and lasted until 4 September 2018, which gave rise to a total of 840  $M_w < 2$  earthquakes (Trionfera 2018; and SISMIKO Group INGV). Before the 16 August mainshock, the study area was hit by two other main events of magnitudes,  $M_w$  4.3 and  $M_w$  4.6 which occurred, respectively, on 25 April 2018 and 14 August 2018 (SISMIKO Group INGV). The two main earthquakes of August 2018 were characterised by hypocentral depths of 19 and 20 km (Bollettino Sismico Italiano INGV).

The Montecilfone seismic sequence struck an area close to the one affected by the 2002 San Giuliano di Puglia seismic sequence (Fig. 1a), located about 20 km south of the Montecilfone epicentral area. Its focal mechanism also indicated a dextral strike-slip rupture, which is consistent with the event of 2002, attributed to the Individual Seismogenic Source ITIS052 (known as San Giuliano di Puglia) and to the Ripabottoni-San Severo Composite Seismogenic Source (ITCS003; DISS Working Group, Fig. 1b), in which rupture took place on the westward prolongation of the Mattinata Fault Zone, about 15 km west of the presumed western end of the  $M_w$  6.7 rupture of 30 July 1627 (corresponding to the ITIS054, San Severo DISS source).

The seismic sequence of 2002 lasted 2 days, since 31 October to 1 November, and consisted of two mainshocks,  $M_w$  5.8 and  $M_w$  5.7. The two seismic events were similar to Montecilfone one in terms of hypocentral depths (ca. 16–20 km) and strike-slip focal mechanisms (Chiarabba et al. 2005; Pondrelli et al. 2006). Interesting similarities about depth and fault-rupture between the San Giuliano di Puglia and Montecilfone earthquakes exist, giving space for more detailed scientific studies.

In the epicentral area of both 2018 and 2002 Molise earthquakes, evidences of past earthquake-induced ground effects are not documented in the CEDIT catalogue (Fig. 1a). Few landslides and ground ruptures are referred to historical 1805 (Sant' Anna), 1627 (Gargano), 1894 (Lesina), and 1980 (Irpinia) earthquakes (Fig. 1a).

The mainshock of 2018 event caused a peak ground acceleration (PGA) up to 0.12 g (<http://shakemap.rm.ingv.it>). Macroseismic surveying was achieved after the main  $M_w$  5.1 event by the INGV QUEST group (Castellano et al. 2018) and MCS intensity values in main localities within the epicentral area were attributed. Limited damages on buildings were registered with a maximum for both MCS and EMS98 scales, with macroseismic grades up to V–VI in Montecilfone, Acquaviva Collecroce, and Castelmauro municipalities. Despite these low values of macroseismic intensity, according to Environmental Seismic Intensity—ESI 2007—scale criteria (Michetti et al. 2007), a higher intensity level, up to VII, can be attributed considering the presence of ground cracks and landslides observed within an area of tens of squared kilometres.

### The 14–17 August 2018 rainfall event

During and after the seismic sequence, the north-eastern part of Molise region was also affected by intense rainfall. The rainfall data recorded by 11 stations operating during the seismic sequence highlighted rainfall values ranged between 120 and 160 mm. Such values have been recorded between 09:00 a.m. UTC of 14 August 2018 and 09:00 a.m. UTC of 17 August 2018; however, in this time interval, two main 24-h sub-events may be distinguished (Table 1). The first one started in the morning of 14 August and was characterised by an average cumulated rainfall of 51.7 mm, even though the stations located in the central part of the study area (i.e. Palata and Guardalfiera-Ponte Liscione) recorded much higher values (81.8 and 77.6 mm respectively). The second sub-event started from the evening of 15 August and the early hours of 16 August, affecting the westernmost part of the study area. This event was characterised by a slightly lower average rainfall intensity (48.2 mm); however, in both cases, quite high 1-h rainfall peaks have been recorded (Table 1). As regards the rainfall cumulated in the 30 days prior to the seismic sequence (15 July—14 August), the resulting values are generally lower than those recorded during the 14–17 August event, except for the data reported by Trivento Station (Table 1), which is, however, one of the farthest stations from the epicentre.

Continuous maps of cumulated rainfalls were derived by IDW method from the recorded data, in order to quantify the spatial distribution of the cumulative rainfall experienced by the epicentral areas and evaluate the role of rainfall as possible trigger or predisposing factor for the landslides surveyed in the epicentral areas (see the “Spatial distribution of triggered ground effects” section).

To evaluate the exceptionality of the above-described rainfall event, a statistical analysis of maximum daily and hourly rainfall intensity data was performed. To this aim, data recorded by Guardalfiera-Ponte Liscione monitoring station, which is the rain gauges closest to the epicentral area, were used. This type of analysis requires sufficiently long and continuous time series of rainfall data (at least 20 years of recorded data according to Houghton et al. 2001 and Serrano 2010) for its reliability; therefore, the Guardalfiera-Ponte Liscione station can be regarded as suitable to perform such an analysis, since it has been recording since 1926. The hydrological–statistical model is based on the analysis of the maximum values assumed by the chosen hydrological variable (i.e. cumulative rainfall at different time intervals). Specifically, we used the generalised extreme value (GEV) distribution (Jenkinson 1955), which is widely used in extreme event frequency analysis rather than the Gumbel distribution, as the literature increasingly suggests that the distribution of extreme events may be more heavily tailed (Fowler and Kilsby 2003). The cumulative distribution function of the GEV distribution is:

$$F(x) = \exp \left\{ - \left( 1 + \xi \frac{x - \mu}{\sigma} \right)^{\frac{1}{\xi}} \right\} \quad (1)$$

where  $\mu$ ,  $\sigma$ , and  $\xi$  are referred to as the location, scale, and shape parameters, respectively. These parameters have been determined by applying the probability weighted moments (PWM) method (Hosking et al. 1985), on the basis of the maximum values of each “cumulative rainfall” variable (i.e. 3, 5, 10, 20, ...180-day rainfall for

**Table 1** Maximum 24-h and 1-h rainfall amounts recorded between 14 and 17 August 2018

Station number	Station name	24-h rainfall (mm)	From	To	1-h rainfall (mm)	From	To
1	Bonefro	46.4	14 August 09:00 am	15 August 09:00 am	35.4	14 August 10:15 am	14 August 11:15 am
2	Castelmauro	68.8	14 August 09:00 am	15 August 09:00 am	22.4	14 August 09:00 am	14 August 10:00 am
3	Lucito	62.6	16 August 01:00 am	17 August 01:00 am	39.8	16 August 01:15 am	16 August 02:15 am
4	Mafalda	56.4	14 August 10:45 am	15 August 10:45 am	39.2	14 August 12:45 pm	14 August 01:45 pm
5	Palata	81.8	14 August 11:00 am	15 August 11:00 am	32.4	14 August 01:30 pm	14 August 02:30 pm
6	Montemitro	66.8	16 August 07:00 am	17 August 07:00 am	20.2	16 August 07:00 am	16 August 08:00 am
7	Guardalfiera-Ponte Liscione	77.6	14 August 10:15 am	15 August 10:15 am	33.6	14 August 11:15 am	14 August 12:15 pm
8	Serra Capriola	7.6	14 August 11:15 am	15 August 11:15 am	4.4	14 August 03:30 pm	14 August 04:30 pm
9	Termoli	23.4	14 August 01:15 pm	15 August 01:15 pm	15.8	14 August 01:15 pm	14 August 02:15 pm
10	Trivento	37.2	15 August 08:45 pm	16 August 08:45 pm	15.6	15 August 08:45 pm	15 August 09:45 pm
11	Civitacampomarano	26.4	16 August 01:30 am	17 August 01:30 am	18.4	16 August 01:30 am	16 August 02:30 am

daily analysis; 1, 3, 6, 12, and 24-h rainfall for hourly analysis) extracted, year by year, from the dataset. Finally, the inversion of the probability function yields the values of cumulated rainfall  $x$  for each of the variables and for different return periods (RPs). Then, these values have been fitted by a power law distribution in order to build the rainfall probability curves.

The resulting daily rainfall probability curves (Fig. 2a) show that the highest RP of maximum rainfall values recorded in August 2018 is equal to 13 years and refers to the shorter duration (i.e. 3 days), while for major periods (such as 30-day cumulated rainfall), the return period is in the order of a few years (Table 2). This evidence suggests that the August 2018 rainfall event cannot be

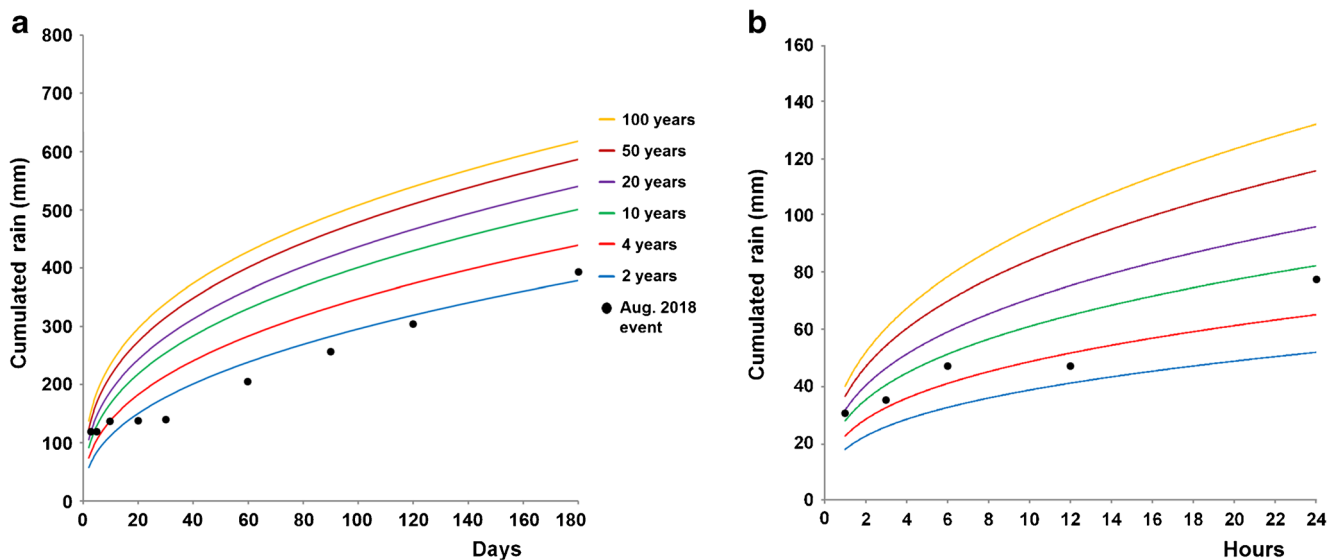


**Fig. 2** Rainfall probability curves for return periods of 2, 4, 10, 20, 50 and 100 years resulting from the historical daily (a) and hourly (b) data recorded at Guardalfiera-Ponte Liscione monitoring station

**Table 2** Computed return period (RP) for the maximum values of rainfall accumulated in time range from 3 to 180 days and from 1 to 24 h according to the data recorded at Guardalfiera-Ponte Liscione station during the August 2018 and January 2003 event

Cumulated days	August 2018 event		January 2003 event	
	Rainfall	RP	Rainfall	RP
3	123.8	13	150	38
5	123.8	9	150	29
10	135.8	4	180	30
20	135.8	< 2	190	11
30	139.2	< 2	201	6
60	205	< 2	311.2	10
90	255.6	< 2	338.4	4
120	303.4	< 2	371.6	5
180	398.2	2	430.4	5
Cumulated hours	Rainfall	RP	Data not available	
1	33.6	17		
3	35	6		
6	47.2	7		
12	47.2	3		
24	77.6	7		

classified as an exceptional event, considering the relatively low RP calculated for each duration. Same conclusions result from hourly rainfall curves (Fig. 2b), albeit the highest RP (which is also in this

case related to the shorter rainfall period, i.e. 1 h) is slightly greater (17 years).

To compare the here considered rainfall scenario with another significant one occurred in the same area and related to similar widespread landsliding conditions, the 24–26 January 2003 rainfall event was also analysed. In that case, thousands of landslides were triggered, generally characterised by reduced thickness and propagation (Fiorillo and Simeone 2004). The RPs of the corresponding rainfall values, which have been estimated through the daily curves, are significantly higher than those obtained for the 2018 event, since they exceed 30 years for duration of 3, 5, and 10 days (Table 2). Even if no hourly data were recorded by the Guardalfiera-Ponte Liscione station on 2003, according to Fiorillo and Simeone (2004), the January 2003 rain storm was quite regularly distributed over several days, with low-intensity peaks, and thus, the landslide occurrence may be related to long-duration/medium-intensity rainfall rather than short-duration/high-intensity rainfall.

**Landslides field surveying and inventorying**

Based on field surveys, 88 earthquake-induced ground effects were detected and classified (Keefer 1984) as 9 disrupted landslides (Fig. 3a), 75 coherent landslides (Fig. 3b), and 4 ground cracks mostly related to slides. The most represented landslide mechanisms are earth slide and earth flow (49 and 15 occurrences, respectively), with only 5% of the failures affecting road cuts (Fig. 3c). The slope angle in correspondence of the landslide areas is homogeneously distributed and ranges between 5° and 40°, with most of the failures occurred between 10° and 15° (Fig. 4a). The latter datum agrees with the type of lithological units outcropping in the study area. Specifically, landslides mainly affected soil cover in gentler

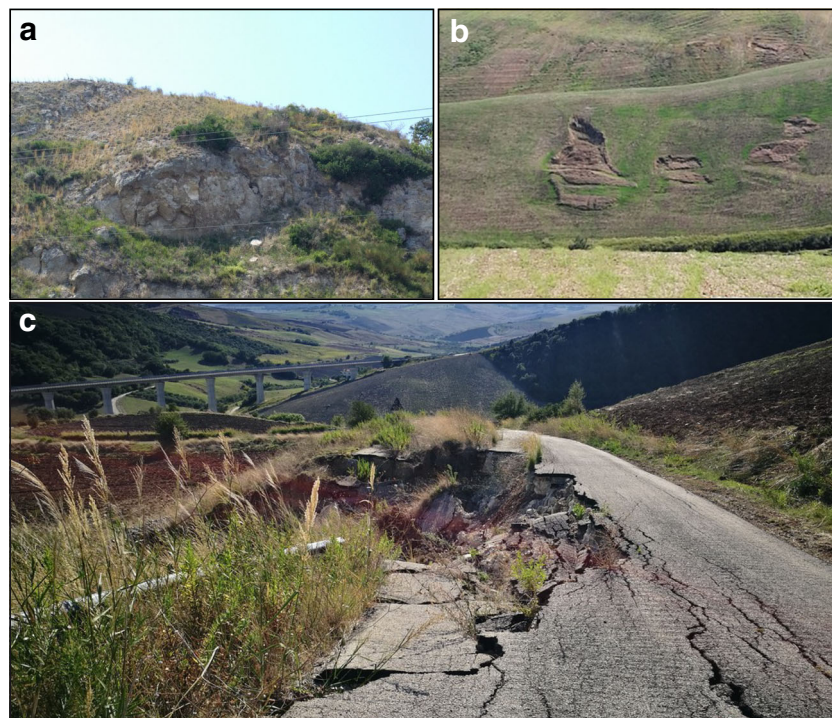


**Fig. 3** Examples of a disrupted and b coherent first-time activation inventoried after the seismic events. Retrogressive reactivation of roto-translational landslides (c) was also highlighted

slopes made up of clays and shales (60%), and only to a lesser extent marls and arenaceous flysch (27%), and alluvial and debris deposits (13%) (Fig. 4b). In this respect, it is worth noticing that the disrupted landslides only affect flysch lithologies with slope angles greater than 26°.

Many of the surveyed earthquake-induced ground effects (up to 37.5%) consisted of reactivated landslides (e.g. in Fig. 3), some of which already catalogued in the official Italian inventory (IFFI - Fig.

4d), while a large proportion correspond to first-time failures on slope. In this sense, pre-earthquake landslide density, which was calculated over a 1–5-km side Fishnet, confirms and testifies the medium-high proneness of the area to slope instability (Fig. 4d).

The surveyed ground effects showed a directional distribution of with a slight NE-SW directivity, corresponding to the main morphostructural alignments (i.e. main drainage network as well as fault systems). Ellipses of directivity revealed a more

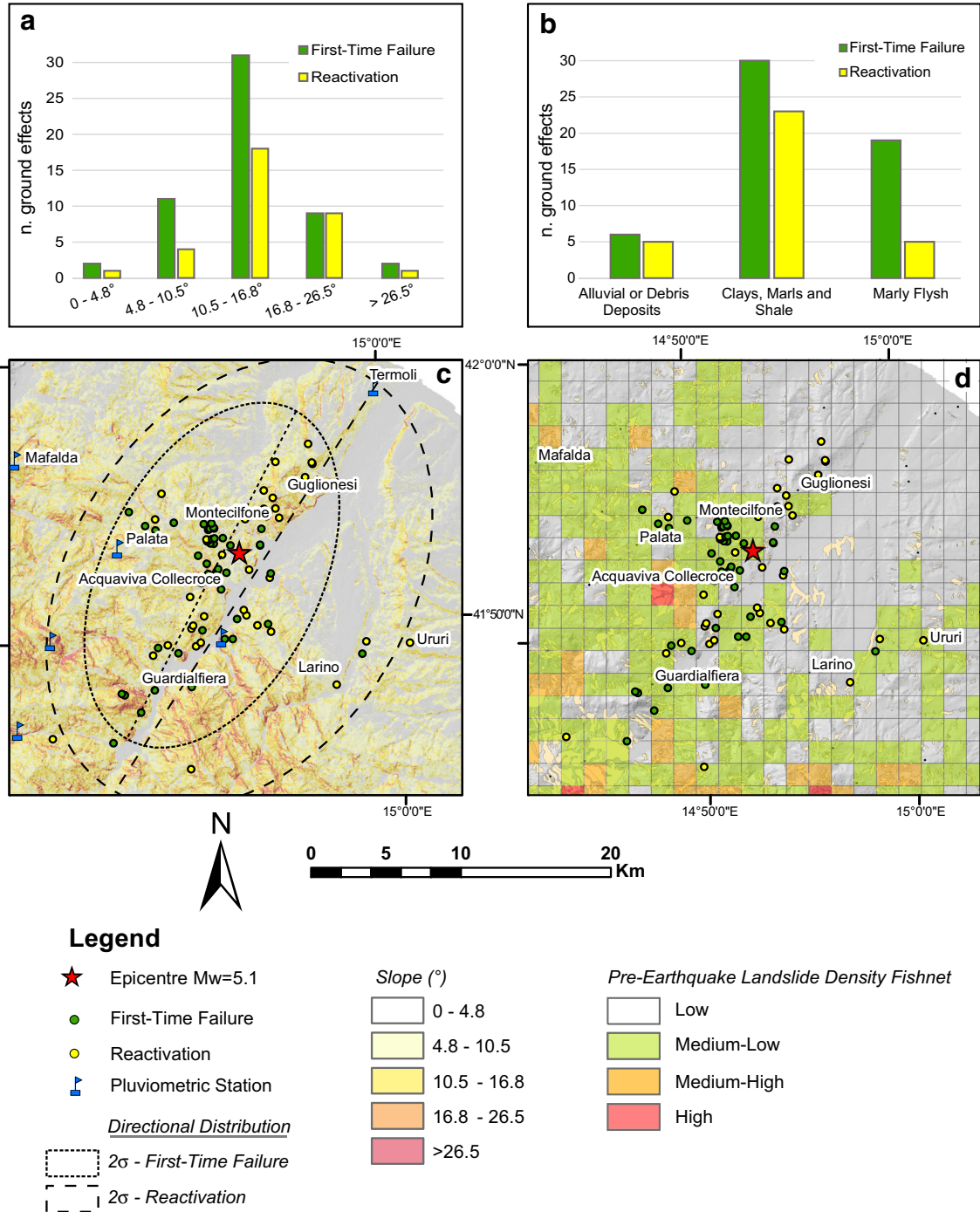


**Fig. 4** Ground effect distribution within slope classes, classified according to natural breaks intervals (a); Jenks 1967, and lithotechnical units (b). Spatial and directional distribution of ground effects show a slight NW-SE directivity, corresponding to the main morphostructural alignments (c). The observed ground effects (yellow and green circles) involve an area characterised by medium-to-high landslide proneness before the earthquake, as revealed by landslide abundance calculated over a regular Fishnet (d)

pronounced direction of first-time failure with respect to landslide reactivations (Fig. 4c).

Regarding the distribution of the earthquake-induced ground effects with respect to the epicentral distance, a typical exponential decay of number of effects with the increasing distance from the epicentre is observed, with maximum distances of occurrence of observed ground effects equal to 7 km for disrupted landslides and up to about 18 km far for coherent landslides (Fig. 5). These distributions were analysed in the following with respect to the intensity of both the triggering factors, trying to derive causative relations with destabilising forces and infer possible single or mutual interactions controlling slope failures.

Based on these data, it results that the totality of disrupted landslides occurred below the distance threshold provided by Keefer (1984) and by Martino et al. (2014) from the CEDIT Italian catalogue for disrupted landslides only (Fig. 6a). On the contrary, 43 out of 75 coherent landslides occurred beyond the maximum expected distance for this mechanism with a  $M_w$  5.1 earthquake fixed at 3.5 km from the epicentre (Fig. 6b). In particular, 25 out of 43 coherent landslides that took place at distance greater than the Keefer threshold were consisted in landslide reactivations, while only 4 out of the remaining 32 occurred below it. This outputs that first-time coherent landslides mainly occurred below the maximum distance provided by the Keefer's curve, while reactivations are predominant at greater epicentral distances, with maximum frequency between 3 and 6 km from epicentre, and frequently consist in earth-slides.

**Spatial distribution of triggered ground effects**

Figure 7a shows the distribution of the ground effects surveyed after the 16 August 2018 Molise earthquake with respect to the seismic action. In particular, the spatial distribution of the surveyed events was analysed taking into account the PGA (g) values provided by the INGV shaking map (<http://shakemap.rm.ingv.it>) that represent the maximum acceleration produced at the ground by the earthquake. The ground effects distribution shows a slightly NE-SW trend, which has no correspondence with the PGA contour lines that showed a linear decrease with distance (Fig. 7a). All the disrupted landslides occurred at higher PGA values (3 effects in 0.075 g and 6 effects in 0.09 g - Fig. 7a). On the contrary, coherent landslides mainly occurred for higher PGA values with 27 effects at 0.09 g (within 4.5 km from the epicentre) and 21 effects at 0.075 g (within 8.5 km from the epicentre). Other 15 coherent effects

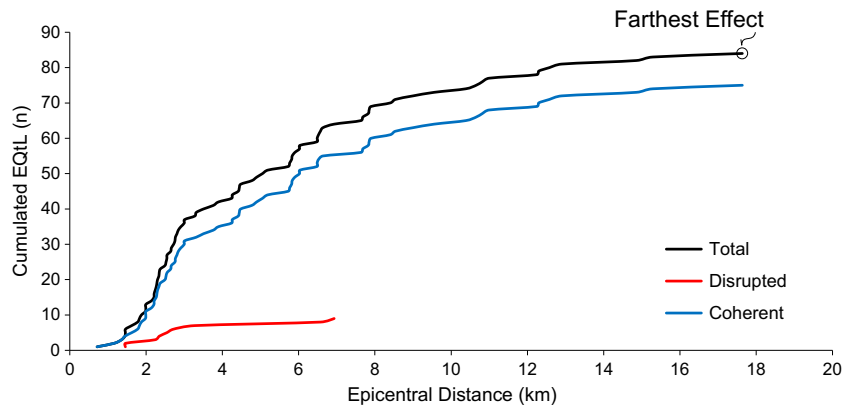


**Fig. 5** Cumulative number of ground effects vs. epicentral distance after the 16 August 2018 Montecilfone earthquake

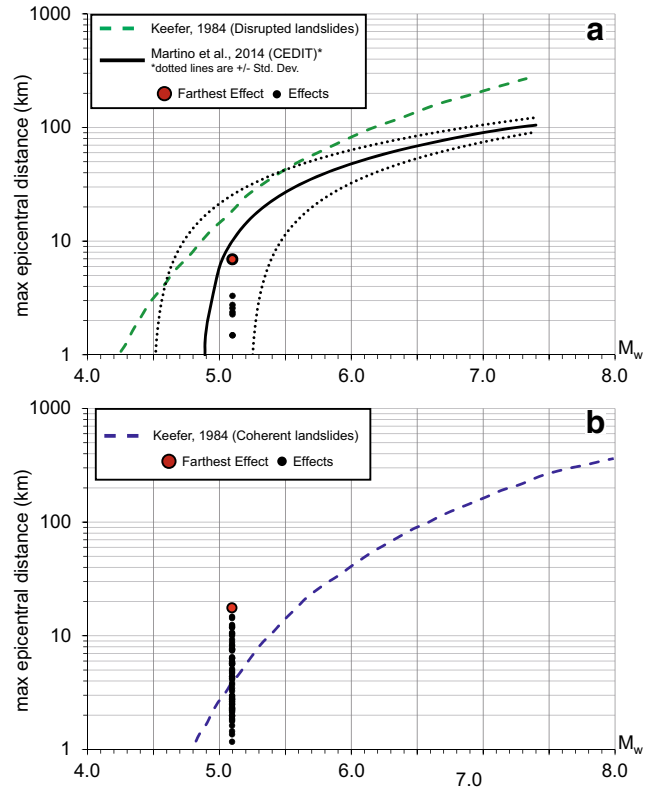


**Fig. 6** Epicentral distance vs. magnitude: comparison among disrupted (a) and coherent (b) landslides, surveyed after Montecilfone EQtL, with respect to literature curves (Keefer 1984)

occurred at lower PGA values within a distance of 10.5 km from the epicentre. To evaluate the seismic damage to the buildings, we also analysed the MCS intensity values for each municipality ([www.questingv.it](http://www.questingv.it)); however, no significant correlation has been derived, given that the distributed proportion of ground effects lies within classes V and VI, with 45 and 37 effects respectively.

The analysis of the spatial distribution of ground effects with respect to the interpolated contours of cumulated rainfall at 17 August 2018 (Fig. 7b) shows that the maximum rainfall values are almost located within the area defined by the Keefer distance for coherent slides, in particular where the intermediate-to-high peak



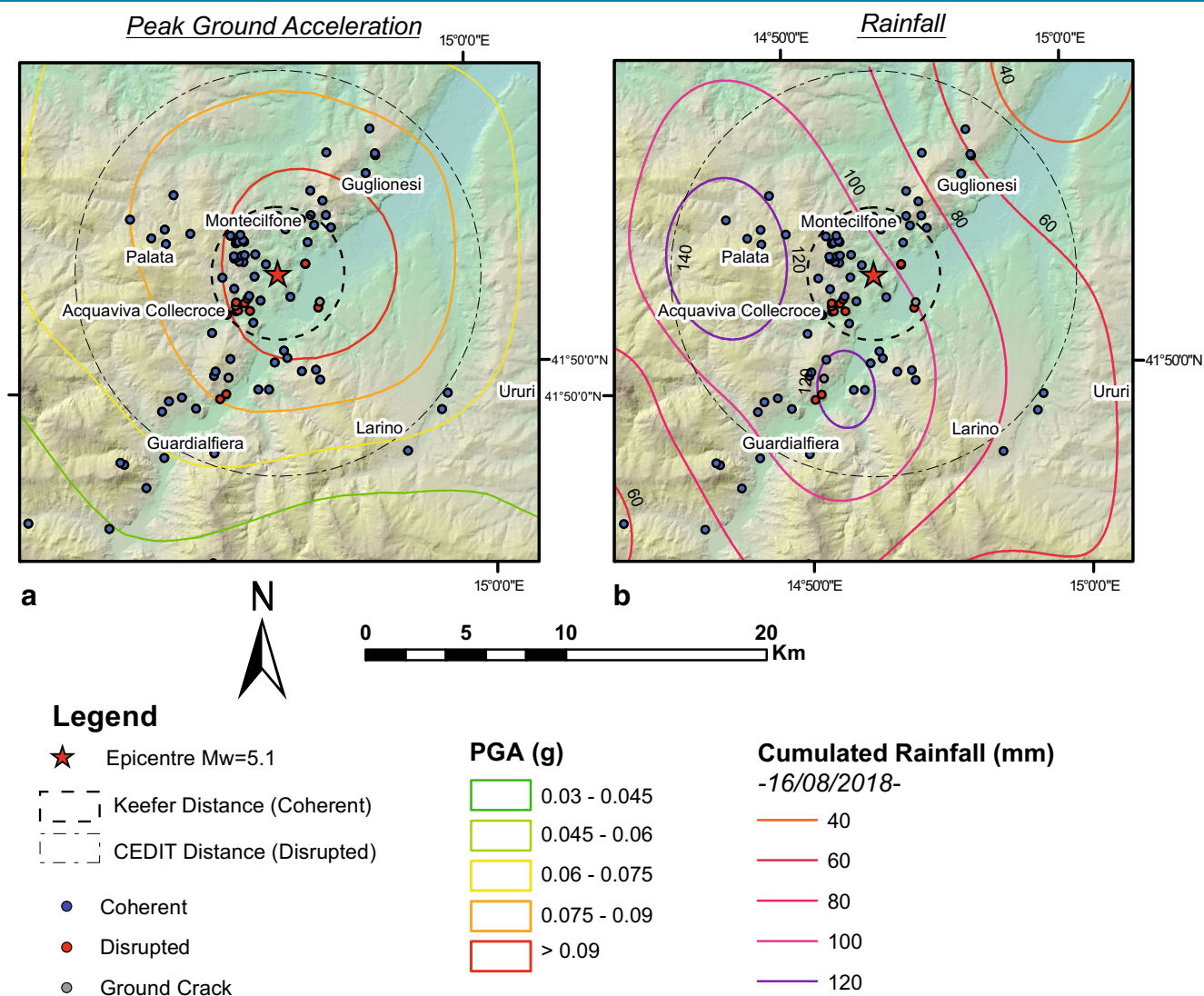


**Fig. 7** Spatial distribution of ground effects surveyed after the 16 August 2018 Montecifone earthquake with respect to a shaking map in PGA (g) (source: [shakemap.rm.ingv.it](http://shakemap.rm.ingv.it)) and b cumulated rainfall at 17 August 2018

of ground acceleration (0.06–0.075 g) shows an offset from inner epicentral areas where the maximum PGA (higher than 0.09 g) was recorded.

The rainfall intensity distribution revealed a slight NW-SE alignment, which is opposite to the one observed for the ground effects (Fig. 7b). The rainfalls experienced in this area occurred in full summer season after a long-lasting period characterised by dry conditions. In fact, according to data, the rainfall cumulated prior to the seismic sequence are generally lower than those recorded during the 14–17 August event, with values varying between 0 and 20 mm in the preceding 30 days (15 July–14 August), and between 0 and 3 mm within 20 days before the seismic event (25 July–14 August).

The combined analysis of intensity values for both the seismic shaking and the rainfall registered in the area where coherent landslides took place highlighted how the maximum number of effects occurred close to the epicentre, i.e. up to 3 km of distance (Fig. 8). Such an area experienced cumulative rainfall up to 110 mm together with the highest range of PGA. In this range of distance,

85% of coherent landslides consist of first-time occurrence, while the remaining 15% are reactivations of pre-existing landslides. Therefore, frequency of first-time failures exponentially decreases with increasing the epicentral distance and decreasing PGA.

This decreasing trend of frequency occurrence for first-time landslides is not directly related with the rainfall event. In fact, some of these effects occurred where maximum values of rainfall and intermediate PGA range are recorded. The coherent landslides that experienced the maximum of rainfalls occurred at epicentral distance greater than the distance expected according to the Keefer curve for coherent landslides, i.e. a distance where the lone role of seismic action (given the  $M_w$ ) should not be sufficient to justify by itself the observed slope failures. In addition, at this distance, the largest number of reactivated landslides with respect to the total was verified, if a distribution for regular distance classes is considered (Fig. 8). Landslide reactivations, in fact, did not show a linear decreasing trend with distance, but rather a bilinear increasing and decreasing trend with a peak of occurrence between 3 and 9 km, where rainfalls higher than 120 mm were recorded (Fig. 8).

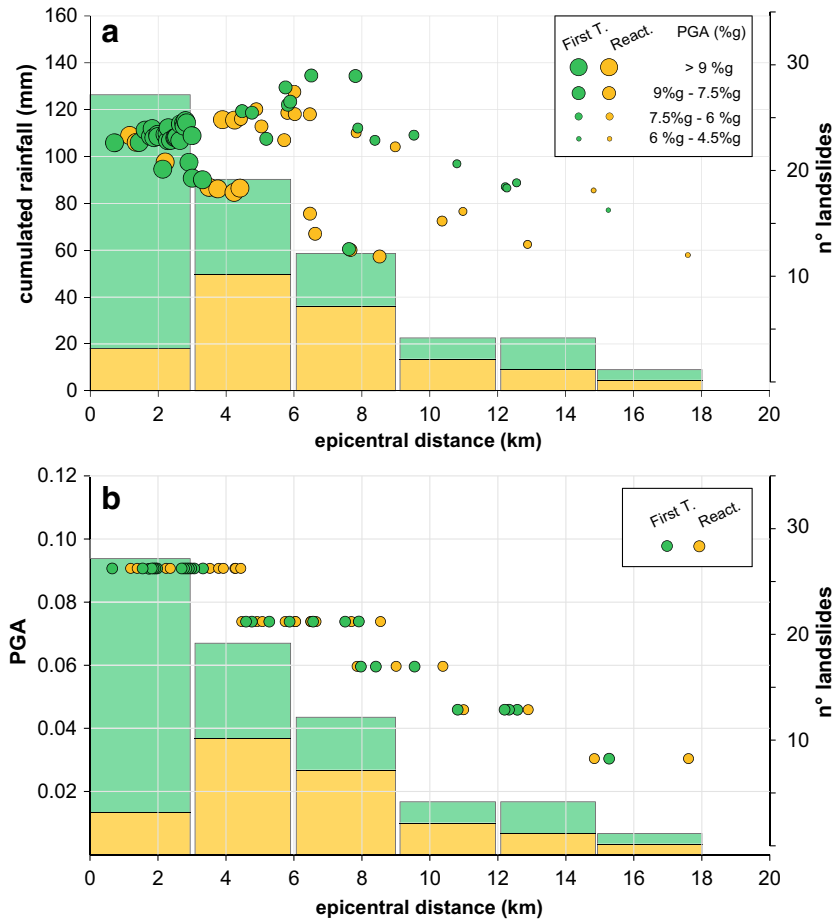


**Fig. 8** Coherent first-time and reactivated landslides distribution related to rainfall (a) and peak ground acceleration—PGA (b)

These evidences suggested how the rainfall played a predominant role in landslide reactivation with respect to the seismic shaking in case of distances higher than the ones provided by the Keefer curve. At distances greater than 9 km, the distributions of both first-time and reactivated landslides follow the observed decrease of PGA, while cumulated rainfalls slightly decrease remaining above 60 mm (Fig. 8). Because of the reduced amount of surveyed disrupted landslides, a similar analysis for this type of landslide could not be performed.

Afterwards, to more rigorously weigh the role of the two destabilising actions in landslides triggering, a landslide density spatial analysis was carried out over a regular 1.5-km-wide squared epicentre-centred fishnet for establishing the concentration of first-time and reactivated landslides with respect to seismic and rainfall inputs. On the basis of the observations resulting from Fig. 9, the spatial distributions of first-time landslides as well as reactivations with respect to both seismic and rainfall action suggest how the occurrence of landslides of coherent type is controlled by the mutual action of the two destabilising factors.

For what it concerns first-time landslides (Fig. 9a), the frequency derived over the all Fishnet's cells significantly shows the maximum and intermediate values (red and orange squares in Fig. 9a) spatially consistent with the PGA maximum values and the expected distances of occurrence for coherent landslides (Keefer 1984). As regards the distribution of landslides reactivations (Fig. 9b), the maximum

abundance of this effects resulted beyond the distance for coherent landslides (Keefer, 1984) in correspondence to the maximum rainfall values and the 0.06–0.075-g PGA range (Fig. 9b). Moreover, it is worth noticing that scattered reactivations and/or first-time landslides can be observed in an independent spatial trend with respect to the analysed destabilising factors all over the study area.

### Discussion

The cross-analysis between landslides, PGA, and rainfall intensity distributions allowed to better describe single or mutual interactions between preparatory and triggering factors able to control slope stability.

As it resulted by the analysis performed on the earthquake-induced ground effects, no peculiar relationship has been found between their spatial distribution and the outcropping lithotechnical units able to justify frequency and distribution; moreover, the effects are homogeneously distributed on the average acclivity of the struck area. These features seem to indicate a lower morphological and geological control on landslides generation when an earthquake occurs.

However, a slight NE-SW alignment of the earthquake-induced ground effects may suggest at least a partial morphostructural control induced by the main physiographic features of the area (e.g. drainage network and fluvial valley), while no trend has been found with respect to the PGA contours.

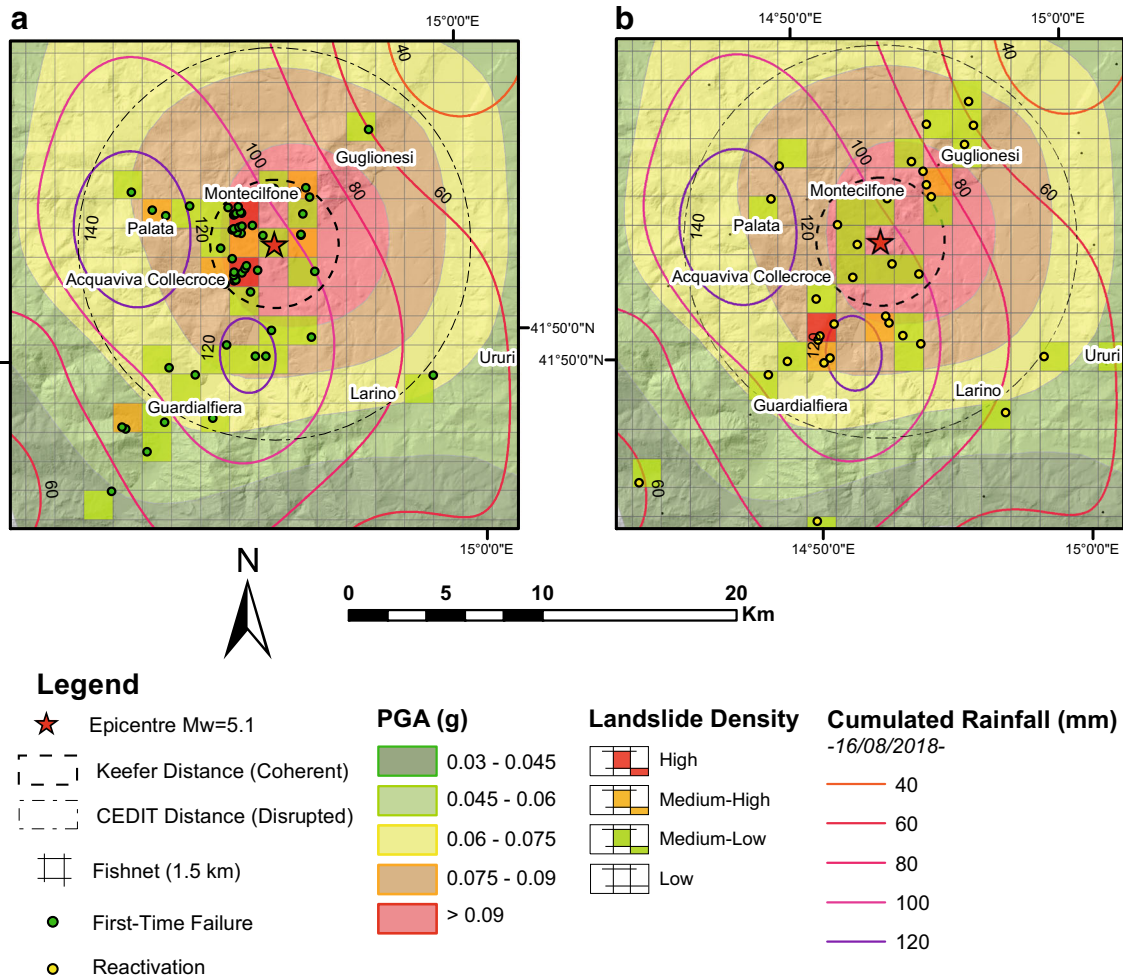


**Fig. 9** Spatial distribution of landslide density derived over a regular squared 1.5-km Fishnet for first-time failures (a) and reactivations (b) with respect to contour lines of PGA and cumulated rainfalls

The observed landslide scenario resulted as the coupled effect of simultaneous destabilising actions (i.e. earthquake and rainfall) which are characterised by different hazard. The lower hazard level can be attributed to the seismic trigger characterised by a return period (RP) between 150 and 200 years, corresponding to a PGA at seismic bedrock of 0.10–0.12 g according to Meletti and Montaldo (2007 - <http://esse1.mi.ingv.it/> - OPCM3519/2006).

Higher hazard was instead derived for the concurrent rainfall event. According to the above-described statistical analysis, it results in maximum RPs of 17 and 13 years referring to a time interval of 1 h and 3 days, respectively (Table 2). Such values, although notable, are significantly lower than RPs derived for the January 2003 rainfall event, during which the triggering of rainfall-induced landslides was documented (Fiorillo and Simeone 2004).

The combined action of earthquake and rainfall results in a lower hazard level, but the contribution of the earthquake appears to be a necessary condition for slope failure. Moreover, the co-seismic-induced effects can also play a control in slope morphological evolution during the post-seismic phase, up to several years after the earthquake (Hovius et al. 2011; Marc et al. 2015), as it could be checked in future.

First-time landslides that occurred within the expected distance according to Keefer's curve are likely referable to the seismic

shaking. On the contrary, first-time occurrence of landslides beyond the Keefer's distance can be retained as the result of the combined action of the two transient processes; in other words, considering their low intensity (also referring to their RP), it is reasonable to assume that they have not been sufficient to induce on their own the observed landslide scenario. In this context, saturation processes occurred within the shallow soils in the days before the seismic event would have given a valuable contribution in the strength reduction where the dynamic stress acted. In this way, the spatial correspondence of rainfall and seismic actions may justify the far-field occurrence of first-time coherent type landslides, i.e. beyond the distance expected according to literature correlations (Keefer 1984; Rodriguez et al. 1999). Such inferences can be supported by slope stability analyses available in literature, which indicate an increase of failure probability exceeding 60% in response to small earthquakes (characterised by low peak ground acceleration values, as in the Montecilfone case) and concurrent rainfalls (Faris and Wang 2014).

The low intensity and the high recurrence of the transient actions which caused the ground failures on August 2018 in the epicentral area of the Montecilfone earthquake, as well as the relative spatial ratio between first-time failure and reactivations

(Fig. 9), suggest as a possible interpretative model for the observed landslide scenario, the jointed aggravating contribution of an earthquake trigger acting on saturated slopes.

Basing on magnitude of seismic action is reasonable to hypothesise that resulting similar landslide scenario cannot be achieved without concurrent rainfall (i.e. dry conditions). Despite this, local primary influence of rainfall in inducing slope failures cannot be excluded.

Although outliers of landslides occurrence with respect to the epicentral distance for disrupted mechanism are more frequently documented to date (mainly due to morphological or anthropic controls; Delgado et al. 2015; Martino et al. 2019), few are the studies dealing with predisposing role of rainfall prior to an earthquake in controlling the spatial trend of coherent failures (Sassa et al. 2007; Wang et al. 2007; Delgado et al. 2011; Jibson and Harp 2012; Fig. 10).

Among these studies, Jibson (1996) and Keefer (2002) reported for the St. George (Utah) earthquake, during which two coherent slides occurred on a clayey slope, saturated by above-ordinary pre-earthquake precipitation were triggered.

Based on these considerations, the here reported EQtL scenario contributes to the catalogue of seismic-induced earthquake-triggered landslides in Italy adding novel information in a zone where no historical data were available so far (Caprari et al. 2018), documenting once again how local geological (Esposito et al. 2000; Bozzano et al. 2001), hydrogeological (Bonilla 1959; Jibson 1996), and morphological (Delgado et al. 2011) features together with local preparatory conditions (Bozzano et al. 2008a, 2008b; Bozzano et al. 2010; Martino et al. 2019) contribute to landslide distribution after earthquakes (Fig. 10).

## Conclusions

The combination of seismic events and heavy rainfalls notoriously drives toward an intensification of landslide-triggered scenarios. However, such combined scenarios have been rarely analysed in terms of mutual weight of the causal factors. One of the reasons relies on the

scarcity of rainfall data and detailed inventories of seismic-induced effects over large areas around the epicentre. The study presented here proposes a combined analysis of the seismic action and the concurrent rainfall to justify the distribution of seismic-induced ground effects following the  $M_w$  5.1 Montecifone (Italy) earthquake. The inventorying and the analyses performed revealed how, with respect to the observed and expected distribution of disrupted landslides, based on maximum distances provided by literature curves (Keefer 1984; Martino et al. 2014), the coherent landslides, instead, involved clayey gently dipping slopes located at much greater distances. This evidence can be explained with the high soil saturation induced by the concurrent intense rainfall event (124 mm of rain in 3 days) that could have aggravated the slope stability conditions resulting in a worse seismically induced scenario. Consequently, if within 10 km from the epicentre the contribution of cumulated rainfall and earthquake shaking cannot be distinguished, at greater distances, the reactivation of earth-slides, against a lower seismic magnitude, can be more distinctly identified as a consequence of the shallow soil saturation.

The analysed landslide catalogue testifies the importance of future studies for a better comprehension of hydrological and soil saturation factors under intense meteo-climatic event in controlling earthquake-induced landslide scenarios at regional scales.

In conclusion, the derived results had better frame the role of combined destabilising/predisposing factors in controlling earthquake-induced ground failures, highlighting as a future perspective a comprehensive quantification of physically based landslide scenarios at regional scales also able to consider potential future climate-related modifications of rainfall occurrence under known and unchanged seismic hazard conditions.

## Acknowledgements

The authors acknowledge P.F. De Pari and the company Geoservizi S.r.l. for the logistic support provided during the field activities. The scientific responsible also thanks the Regione Molise Civil Protection Agency and A. Cardillo and S. Di Pilla for providing the rainfall data.

## Authors contributions

In the present study, S. Martino was the scientific responsible of the research group. F. Bozzano and C. Esposito coordinated specific research activities and contributed to pre-processing. B. Antonielli, P. Caprari, M.E. Discenza, M. Fiorucci, and R. Iannucci performed field surveys and data acquisition. L. Schilirò completed the statistical analysis of historical rainfall data and analysed the rainfall event. M. Fiorucci and G.M. Marmoni performed the geospatial and statistical analyses and contributed to the geo-database management and post-processing. All authors contributed to the interpretation of results and to the manuscript writing.

## Funding information

The Research Centre for Geological Risks (CERI) of the University of Rome "Sapienza" funded the field surveys and activities.

## References

Alfaro P, Delgado J, García-Tortosa FJ, Lenti L, Lopez JA, Lopez-Casado C, Martino S (2012) Widespread landslides induced by the  $M_w$  5.1 earthquake of 11 May 2011 in Lorca, SE Spain. Eng Geol 137-138:40–52

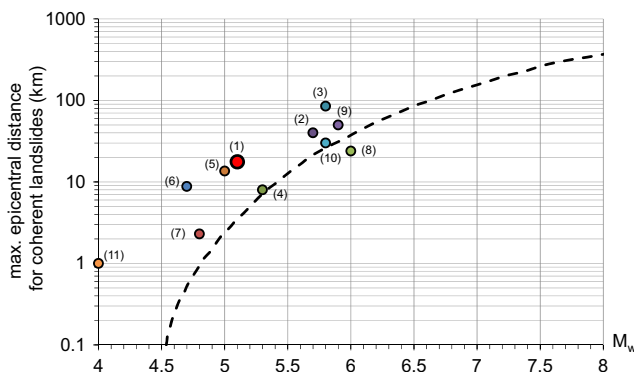


**Fig. 10** Catalogue of maximum epicentral distance for coherent landslides exceeding the dashed curve by Keefer (1984); (1) 2018 Montecifone Earthquake (this study); (2) 1992 San Giorgio Utah (Jibson 1996); (3) 1988 Quebec (Rodriguez et al. 1999); (4) 1957 Daly city (Bonilla 1959); (5) 1984 W Lentegi (Delgado et al. 2011); (6) 1999 N Mula (Delgado et al. 2011); (7) 1964 SW Galera (Delgado et al. 2011); (8) 1997 Umbria-Marche (Esposito et al. 2000; Bozzano et al. 2001); (9) 2002 Palermo (Bozzano et al. 2008a); (10) 2002 San Giuliano Puglia (Bozzano et al. 2008b); (11) 2017 Ischia (Caprari et al. 2018)

- APAT (2007). Report on landslides in Italy: the IFFI project. Methodology, results and regional reports. APAT Reports 78:681
- Ascione A, Cinque A, Miccadei E, Villani F, Berti C (2008) The Plio-Quaternary uplift of the Apennine chain: new data from the analysis of topography and river valleys in Central Italy. *Geomorphology* 102:105–118
- Aucelli PPC, Cinque A, Roszkopf CM (2001) Geomorphological map of the Trigno basin (Italy): explanation notes. *Geogr Fis Dinam Quat* 24:3–12
- Aucelli PPC, Iannantuono E, Roszkopf CM (2009) Recent evolution and risk of erosion of the Molise coast (Southern Italy). *Bollettino della Società Geologica Italiana* 128:759–771
- Bonilla MG (1959) Geologic observation in the epicentral area of the San Francisco earthquake of March 22, 1957. In: San Francisco Earthquake of March 1957: California Div. Mines and Geology Spec. Rept no 57, pp 25–37
- Borgomeo E, Hebditch KV, Whittaker AC, Loneragan L (2014) Characterising the spatial distribution, frequency and geomorphic controls on landslide occurrence, Molise, Italy. *Geomorphology* 226:148–161
- Bozzano F, Cardarelli E, Cercato M, Lenti L, Martino S, Paciello A, Scarascia Mugnozza G (2008a) Engineering-geology model of the seismically-induced Cerda landslide (Sicily, Italy). *Boll Geofis Teor Appl* 49(2):205–225
- Bozzano F, Gambino P, Larosa I, Scarascia Mugnozza G (2001) Analisi preliminare degli effetti di superficie indotti dalla sequenza sismica umbro-marchigiana nei mesi di settembre-ottobre 1997. *Mem Soc Geol Ital* 56:283–290
- Bozzano F, Lenti L, Martino S, Paciello A, Scarascia Mugnozza G (2008b) Self-excitation process due to local seismic amplification responsible for the reactivation of the Salcito landslide (Italy) on 31 October 2002. *J Geophys Res* 113:B10312. <https://doi.org/10.1029/2007JB005309>
- Bozzano F, Lenti L, Martino S, Paciello A, Scarascia Mugnozza G (2010) Evidences of landslide earthquake triggering due to self-excitation process. *Int J Earth Sci* 100:861–879. <https://doi.org/10.1007/s00531-010-0514-5>
- Calamita F, Satolli S, Scisciani V, Esestima P, Pace P (2011) Contrasting styles of fault reactivation in curved orogenic belts: examples from the Central Apennines (Italy). *Geol Soc Am Bull* 123(5):1097–1111
- Caprari P, Della Seta M, Martino S, Fantini A, Fiorucci M, Priore T (2018) Upgrade of the CEDIT database of earthquake-induced ground effects in Italy. *Italian Journal of Engineering Geology and Environment* 2:23–39. <https://doi.org/10.4408/IJEGE.2018-02.0-02>
- Casnedi R (1978) Pliocene sedimentation and tectonics in the lower part of the Lower Valle del Fortore (Foggia). *Mem Soc Geol Ital* 19:605–612
- Castellano C, Del Mese S, Fodarella A, Graziani L, Maramai A, Tertuliani A, Verrubbi V (2018) QUEST- Rilievo macrosismico per i terremoti del Molise del 14 e 16 agosto 2018, rapporto interno INGV. <https://doi.org/10.5281/zenodo.1405385>
- Chiarabba C, De Gori P, Chiaraluce L, Bordoni P, Cattaneo M, De Martin M, Frepoli A, Michelini A, Monachesi A, Moretti M, Augliera GP, D'Alema E, Frapiccini M, Gassi A, Marzorati S, Di Bartolomeo P, Gentile S, Govoni A, Lovisa L, Romanelli M, Ferretti G, Pasta M, Spallarossa D, Zunino E (2005) Mainshocks and aftershocks of the 2002 Molise seismic sequence, southern Italy. *J Seismol* 9(4):487–494
- Ciaranfi N, Guida M, Iaccarino G, Pescatore T, Pieri P, Rapidarsi L, Ricchetti G, Sgrosso I, Torre M, Tortorici L, Turco E, Scarpa R, Cuscito M, Guerra I, Iannaccone G, Panza GF, Scandone P (1983) Seismotectonic elements of the southern Apennines. *Bollettino della Società Geologica Italiana* 102:201–222
- Ciaranfi N, Pieri P, Ricchetti G (1988) Notes to the geological map of the Murge and of the Salento (Central-Southern Puglia). *Mem Soc Geol Ital* 41:449–460
- Cinque A, Patacca E, Scandone P, Tozzi M (1993) Quaternary kinematic evolution of the Southern Apennines. Relationships between surface geological features and deep lithospheric structures. *Annals of Geophysics* 36:121–142
- Corrado S, Di Bucci D, Leschiutta I, Naso G, Trigari A (1997) The quaternary tectonics of the Isernia plain in the structural evolution of the Molise sector. *Il Quaternario* 10:609–614
- Crozier MJ (2005) Multiple-occurrence regional landslide events in New Zealand: hazard management issues. *Landslides* 2:247–256
- Delgado J, García-Tortosa FJ, Garrido J, Loffredo A, López-Casado C, Martín-Rojas I, Rodríguez-Peces MJ (2015) Seismically-induced landslides by a low-magnitude earthquake: the  $M_w$ 4.7 Ossa De Montiel event (central Spain). *Eng Geo* 196:280–285. <https://doi.org/10.1016/j.enggeo.2015.07.016>
- Delgado J, Garrido J, López-Casado C, Martino S, Peláez JA (2011) On far field occurrence of seismically induced landslides. *Eng Geol* 123(3):04–213. <https://doi.org/10.1016/j.enggeo.2011.08.002>
- Del Gaudio V, Muscillo S, Wasowski J (2014) What we can learn about slope response to earthquakes from ambient noise analysis: an overview. *Eng Geol* 182:182–200
- Della Seta M, Martino S, Scarascia Mugnozza G (2013) Quaternary sea-level change and slope instability in coastal areas: insights from the Vasto landslide (Adriatic coast, central Italy). *Geomorphology* 201:462–478
- Di Bucci D, Corrado S, Naso G, Parotto M, Pratluron A (1999) Neogenic-quaternary tectonic evolution of the Molise area. *Bollettino della Società Geologica Italiana* 118:13–30
- DISS Working group (2018) Database of Individual Seismogenic Sources (DISS), version 3.2.1: a compilation of potential sources for earthquakes larger than M 5.5 in Italy and surrounding areas. (<http://diss.rm.ingv.it/diss/>). Istituto Nazionale di Geofisica e Vulcanologia
- Dogliani C, Mongelli F, Pieri P (1994) The Puglia uplift (SE Italy): an anomaly in the foreland of the Apenninic subduction due to buckling of a thick continental lithosphere. *Tectonics* 13:1309–1321
- Esposito E, Porfido S, Simonelli AL, Mastrolorenzo G, Iaccarino G (2000) Landslides and other surface effects induced by the 1997 Umbria–Marche seismic sequence. *Eng Geol* 58:353–376
- Fan X, Scaringi G, Korup O, West AJ, van Westen CJ, Tanya H, Hovius N, Hales T, Jibson RW, Allstadt KE, Zhang L, Evans SG, Chong X, Li G, Pei X, Xu Q, Huang R (2019) Earthquake-induced chains of geologic hazards: patterns, mechanisms, and impacts. *Rev Geophys* 57(2):421–503
- Faris F, Wang F (2014) Stochastic analysis of rainfall effect on earthquake induced shallow landslide of Tandikat, West Sumatra, Indonesia. *Geoenvironmental Disasters* 1(1):12–13. <https://doi.org/10.1186/s40677-014-0012-3>
- Fiorillo F (2003) Geological features and landslide mechanisms of an unstable coastal slope (Petacciato, Italy). *Eng Geol* 67:255–267
- Fiorillo F, Simeone V (2004) Analysis of rainfall in landslide activation during January–February 2003 in central-south-eastern Italy. Balwois 2004 - Conference on Water Observation and Information System for Decision Support, Ohrid, Macedonia, 25–29 May 2004: 7 pp.
- Fortunato C, Martino S, Prestinanzi A, Romeo RW, Fantini A, Sarandrea P (2012) New release of the Italian catalogue of earthquake-induced ground failures (CEDIT). *Italian Journal of Engineering Geology and Environment* 2:63–74
- Fowler HJ, Kilsby CG (2003) A regional frequency analysis of United Kingdom extreme rainfall from 1961 to 2000. *Int J Climatol* 23:1313–1334. <https://doi.org/10.1002/joc.943>
- Gambini R, Tozzi M (1996) Tertiary geodynamic evolution of the southern Adria microplate. *Terra Nova* 8:593–602
- Gorum T, Carranza EJM (2015) Control of style-of-faulting on spatial pattern of earthquake-triggered landslides. *Int J Environ Sci Technol* 12(10):3189–3212. <https://doi.org/10.1007/s13762-015-0752-y>
- Gorum T, Korup O, van Westen CJ, van der Meijde M, Xu C, van der Meer FD (2014) Why so few? Landslides triggered by the 2002 Denali earthquake, Alaska. *Quat Sci Rev* 95:80–94. <https://doi.org/10.1016/j.quascirev.2014.04.032>
- Hosking JRM, Wallis JR, Wood EF (1985) Estimation of the generalized extreme value distribution by the method of probability weighted moments. *Technometrics* 27:251–261. <https://doi.org/10.1080/00401706.1985.10488049>
- Houghton JT, Ding Y, Griggs DJ, Noguera M, van der Linden PJ, Dai X, Maskell K, Johnson CA (2001) Climate change 2001: the scientific basis. Contribution of working group I to the third assessment report of the intergovernmental panel on climate change. Cambridge University Press, Cambridge, UK/New York, USA, 881 pp
- Hovius N, Meunier P, Lin CW, Chen H, Chen YG, Dadson S, Ming-Jame H, Lines M (2011) Prolonged seismically induced erosion and the mass balance of a large earthquake. *Earth Planet Sci Lett* 304(3–4):347–355. <https://doi.org/10.1016/j.epsl.2011.02.005>
- Hungr O, Leroueil S, Picarelli L (2014) The Varnes classification of landslide types, an update. *Landslides* 11:167–194
- Hutchinson JN (1988) General report: morphological and geotechnical parameters of landslides in relation to geology and hydrogeology. In: Bonnard C (ed) Proceedings of the fifth international symposium on landslides, vol 1. Balkema, Rotterdam, pp 3–35
- Jenkinson AF (1955) The frequency distribution of the annual maximum (or minimum) values of meteorological events. *Q J Royal Meteorol Soc* 87:158–171. <https://doi.org/10.1002/qj.49708134804>
- Jenks GF (1967) The data model concept in statistical mapping. *International Yearbook of Cartography* 7:186–190
- Jibson RW (1993) Predicting earthquake-induced landslide displacements using Newmark's sliding block analysis. *Transport Res Rec* 1411:9–17
- Jibson RW (1996) Use of landslides for paleoseismic analysis. *Eng Geol* 43(4):291–323
- Jibson RW (2007) Regression models for estimating coseismic landslide displacement. *Eng Geol* 91(2–4):209–218. <https://doi.org/10.1016/j.enggeo.2007.01.013>

- Jibson RW, Harp EL (2012) Extraordinary distance limits of landslides triggered by the 2011 mineral, Virginia, earthquake. *Bull Seismol Soc Am* 102(6):2368–2377. <https://doi.org/10.1785/0120120055>
- Keefer DK (1984) Landslides caused by earthquakes. *Geol Soc Am Bull* 95(4):406. [https://doi.org/10.1130/0016-7606\(1984\)95<406:LCBE>2.0.CO;2](https://doi.org/10.1130/0016-7606(1984)95<406:LCBE>2.0.CO;2)
- Keefer DK (2002) Investigating landslides caused by earthquakes - a historical review. *Surv Geophys* 23(6):473–510. <https://doi.org/10.1023/A:1021274710840>
- Malamud BD, Turcotte DL, Guzzetti F, Reichenbach P (2004) Landslides, earthquakes, and erosion. *Earth Planet Sci Lett* 229(1–2):45–59. <https://doi.org/10.1016/j.epsl.2004.10.018>
- Marc O, Hovius N, Meunier P, Uchida T, Hayashi S (2015) Transient changes of landslide rates after earthquakes. *Geology* 43(10):883–886. <https://doi.org/10.1130/G36961.1>
- Martino S, Prestininzi A, Romeo RW (2014) Earthquake-induced ground failures in Italy from a reviewed database. *Nat Hazards Earth Syst Sci* 14:799–814
- Martino S, Lenti L, Delgado J, Garrido J, Lopez-Casado C (2016) Application of a characteristic periods-based (CPB) approach to estimate earthquake-induced displacements of landslides through dynamic numerical modelling. *Geophys J Int* 206:82–102
- Martino S, Bozzano F, Caporossi P, D'Angiò D, Della Seta M, Esposito C, Fantini A, Fiorucci M, Giannini LM, Iannucci R, Marmoni GM, Mazzanti P, Missori C, Moretto S, Rivellino S, Romeo RW, Sarandrea P, Schilirò L, Troiani F, Varone C (2017) Ground effects triggered by the August 24th 2016, Mw 6.0 Amatrice (Italy) earthquake: survey and inventorying to update the CEDIT catalogue. *Geogr Fis Dinam Quat* 40:77–95
- Martino S, Bozzano F, Caporossi P, D'Angiò D, Della Seta M, Esposito C, Fantini A, Fiorucci M, Giannini LM, Iannucci R, Marmoni GM, Mazzanti P, Missori C, Moretto S, Piacentini D, Rivellino S, Romeo RW, Sarandrea P, Schilirò L, Troiani F, Varone C (2019) Impact of landslides on transportation routes during the 2016–2017 Central Italy seismic sequence. *Landslides* 16(6):1221–1241. <https://doi.org/10.1007/s10346-019-01162-2>
- Meletti C, Montaldo V (2007) Stime di pericolosità sismica per diverse probabilità di superamento in 50 anni: valori di ag. Progetto DPC-INGV S1, Deliverable D2, <http://esse1.mi.ingv.it/d2.html>
- Meunier P, Hovius N, Haines AJ (2007) Regional patterns of earthquake-triggered landslides and their relation to ground motion. *Geophys Res Lett* 34:L20408. <https://doi.org/10.1029/2007GL031337>
- Miccadei E, Mascioli F, Ricci F, Piacentini T (2019) Geomorphology of soft clastic rock coasts in the mid-western Adriatic Sea (Abruzzo, Italy). *Geomorphology* 324:72–94
- Michetti AM, Esposito E, Guerrieri L, Porfido S, Serva L, Tatevossian R, Vittori E, Audemard F, Azuma T, Clague J, Comerci V, Gürpınar A, Mc Calpin J, Mohammadioun B, Mörner NA, Ota Y, Roghoozi E (2007) Environmental Seismic Intensity scale - ESI 2007 La scala di Intensità Sismica basata sugli effetti ambientali - ESI 2007. Memorie descrittive della carta geologica D'Italia. LXXIV, APAT
- Nowicki MA, Wald DJ, Hamburger MW, Hearne M, Thompson EM (2014) Development of a globally applicable model for near real-time prediction of seismically induced landslides. *Eng Geol* 173:54–65. <https://doi.org/10.1016/j.enggeo.2014.02.002>
- Parotto M, Praturlon A (2004) The southern Apennine arc. In: *Geology of Italy. Special Value of the Italian Geological Society for the IGC 32*, Florence, 53–58
- Patacca E, Scandone P, Bellatalla M, Perilli N, Santini U (1992) The junction area between the northern Apennine arch and the southern Apennine arc in Abruzzo and Molise. *Studi Geol Camerti* 1991(92):417–441
- Patacca E, Scandone P (2007) Geology of the Southern Apennines. *Bollettino della Società Geologica Italiana* 7:75–119
- Pisano L, Zumpano V, Dragone V, Parise M (2017) Built-up area exposure to landslides and related social impacts in Molise (Italy). 4th World Landslide Forum, Ljubljana, Slovenia
- Pondrelli S, Salimbeni S, Ekstrom G, Morelli A, Gasperini P, Vannucci G (2006) The Italian CMT dataset from 1977 to the present. *Phys Earth Planet* 159(3–4):286–303
- Rapisardi L (1978) Neotectonic features on the Molise-Abruzzo border. *Applied Geology and Hydrogeology* 13:223–232
- Ricchetti G, Ciaranfi N, Luperto Sinni E, Mongelli F, Pieri P (1988) Geodynamics and sedimentary and tectonic evolution of the Apulian foreland. *Mem Soc Geol Ital* 41:57–82
- Rodríguez CE, Bommer JJ, Chandler RJ (1999) Earthquake-induced landslides: 1980–1997. *Soil Dyn Earthq Eng* 18:325–346
- Roskopf CM, Scorpio V (2013) Geomorphologic map of the Biferno River valley floor system (Molise, southern Italy). *Journal of Maps* 9(1):106–114. <https://doi.org/10.1080/17530350.2012.755385>
- Rovida A, Locati M, Camassi R, Lolli B, Gasperini P (2016) CPTI15, the 2015 version of the parametric catalogue of Italian earthquakes. Milano, Bologna). <https://doi.org/10.6092/INGV.IT-CPTI15>. <http://emidius.mi.ingv.it/CPTI>
- Sassa K, Fukuoka H, Wang F, Wang G (2007) Landslides induced by a combined effect of earthquake and rainfall. In: *Progress in landslide science*. Springer, Berlin, Heidelberg, pp 193–207
- Scrocca D, Tozzi M (1999) Mio-Pliocene Tectogenesis of the Molise Apennines. *Bollettino della Società Geologica Italiana* 118:255–286
- Serrano SE (2010) Hydrology for engineers, geologists, and environmental professionals: an integrated treatment of surface, subsurface, and contaminant hydrology, Second edn. Hydroscience Inc., USA, 590 pp
- Spalluto L, Moretti M (2006) Evidence of neotectonic (Middle Pliocene - Upper Pleistocene) in the western sector of the Gargano Promontory (Southern Italy). *Il Quaternario* 19:143–154
- Suwa H (2006) Catastrophe caused by the 17 February 2006 Southern Leyte landslide in Philippine. *Natural Disaster Science* 25(1):83–97 (in Japanese)
- Tanyas H, van Westen CJ, Allstadt KE, Anna Nowicki Jessee M, Görüm T, Jibson RW, Godt JW, Sato HP, Schmitt RG, Marc O, Hovius N (2017) Presentation and analysis of a worldwide database of earthquake-induced landslide inventories: earthquake-induced landslide inventories. *J Geophys Res Earth Surf* 122:1991–2015. <https://doi.org/10.1002/2017JF004236>
- Trionfera B (2018) Analisi della sismicità del Molise nel periodo 2013–2018 e considerazioni geodinamiche (in Italian). Master Thesis. Advisor Prof. Carlo Doglioni
- Valagussa A, Marc O, Frattini P, Crosta GB (2019) Seismic and geological controls on earthquake-induced landslide size. *Earth Planet Sci Lett* 506:268–281. <https://doi.org/10.1016/j.epsl.2018.11.005>
- Vezzani L, Festa A, Ghisetti F (2010) Geology and tectonic evolution of the Central-Southern Apennines, Italy. *Geological Society of America Special Paper* 469. <https://doi.org/10.1130/SPE469>
- Vezzani L, Ghisetti F, Festa A (2004) Geological map of Molise (scale 1: 100000). S.E.L.CA
- Wang HB, Sassa K, Xu WY (2007) Analysis of a spatial distribution of landslides triggered by the 2004 Chuetsu earthquakes of Niigata Prefecture, Japan. *Nat Hazards* 41(1):43–60. <https://doi.org/10.1007/s11069-006-9009-x>

S. Martino  · B. Antonielli · F. Bozzano · P. Caprari · C. Esposito · M. Fiorucci · R. Iannucci · G. Marmoni · L. Schilirò

Department of Earth Sciences and Research Centre for Geological Risks (CERI), University of Rome "Sapienza", Rome, Italy  
Email: salvatore.martino@uniroma1.it

M. E. Discenza

Geoservizi S.r.l. - Engineering Integrated Systems, Ripalimosani, Campobasso, Italy